Chemical Physics 406 (2012) 3–8

Contents lists available at SciVerse ScienceDirect

Chemical Physics

journal homepage: www.elsevier.com/locate/chemphys

Fluorescence correlation spectroscopy at high concentrations using gold bowtie nanoantennas

Anika A. Kinkhabwala [a,b], Zongfu Yu [c], Shanhui Fan [c], W.E. Moerner [a,*]

[a] Department of Chemistry, Stanford University, USA
[b] Department of Applied Physics, Stanford University, USA
[c] Department of Electrical Engineering, Stanford University, USA

ARTICLE INFO

Article history:
Available online 21 April 2012

Keywords:
Plasmonics
FCS
Single-molecule
Fluorescence
Nanophotonics

ABSTRACT

Fluorescence correlation spectroscopy (FCS) measures the fluorescence fluctuations of fluorophores in solution, but is restricted to extremely low concentrations. Plasmonic gold bowtie nanoantennas enhance a single molecule's fluorescence relative to a large background of unenhanced molecules, and here we show that bowties can extend FCS measurements to much higher concentrations. In this demonstration, the bowtie-FCS signal is dominated by molecules that transiently stick to the substrate near the bowtie gap, and photobleaching/photoblinking dynamics for two fluorophores are measured on the 10–100 ms time scale.

In a typical fluorescence correlation spectroscopy (FCS) experiment, a laser beam is focused into a dilute solution of fluorescent molecules forming a very small elongated Gaussian-shaped focal volume. A confocal fluorescence microscope then measures the bright flashes of fluorescence from small numbers or single molecules passing through the diffraction-limited focused laser spot of transverse diameter ~250 nm in the visible. The autocorrelation of the fluorescence time trace provides information on any dynamics in the fluorescence signal on time scales shorter than the diffusion time through the laser focus (typically O(1 ms)) [1–3]. Examples of processes that affect fluorescence on these time scales are photon antibunching, dark state bottlenecks, photobleaching, conformational dynamics, FRET, and diffusion; these types of measurements have been performed on a number of free dye and labeled biological systems including fluorescent proteins [4] yielding a wealth of information. By exact analysis of the optical configuration, even absolute diffusion coefficients may be extracted [5]. FCS is performed at low dye concentrations so that the bursts of fluorescence from single molecule have maximum contrast, but this limits the technique to solutions of 10 pM–1 nM concentrations [6].

It was recently demonstrated that high concentration FCS experiments can be performed by using zero-mode waveguides to confine the illumination volume much further than is possible with normal diffraction-limited confocal microscopy [7]. Zero-mode waveguides consist of subwavelength diameter (~70–100 nm) holes in thin aluminum films. Electromagnetic waves cannot propagate through subwavelength holes, so there is only a weak penetration of evanescent waves into these apertures, restricting illumination to a few 10s of nm from the substrate. This technique allows FCS experiments in solutions with concentrations as high as 200 μM [7]. This scheme has enabled real-time single-molecule sequencing of DNA [8], as well as real-time translation of RNA into protein [9].

Plasmonic nanoantennas can be used to concentrate and enhance electromagnetic fields at optical frequencies [10] allowing for enhancement of light-molecule interactions in these localized electromagnetic fields. In particular, gold bowtie nanoantennas, which enhance local $|E|^2$ fields by factors up to 1000 [11] in a $\sim(20\text{ nm})^3$ region, have been shown to enhance a single-molecule's fluorescence by factors up to 1300 [12]. Zero-mode waveguides, however, have only been shown to enhance fluorescence up to 25× [13–16]. The bowtie structure, being lithographically fabricated, allows the generation of large arrays of repeatable structures, as opposed to studies utilizing localized surface plasmons in gold colloidal particles as the antenna [17]. This paper demonstrates that bowtie nanoantennas can be used for single-molecule experiments in high concentration solutions and shows that the enhanced signal is from molecules nonspecifically stuck to the surface near the bowtie, not from diffusing molecules. The extension of these ideas to specifically attached molecules or molecules which bind near the bowtie by molecular interactions is clear. The demonstration experiment described here consists of immersing bowtie nanoantennas into concentrated dye solutions and

* Corresponding author. Address: Department of Chemistry, Mail Code 5080, Stanford University, Stanford, CA 94305-5080, USA. Tel.: +1 650 723 1727; fax: +1 650 725 0259.
E-mail address: wmoerner@stanford.edu (W.E. Moerner).

0301-0104/$ - see front matter © 2012 Elsevier B.V. All rights reserved.
http://dx.doi.org/10.1016/j.chemphys.2012.04.011

measuring the fluorescence bursts and fluctuations from molecules near the bowties using an inverted confocal fluorescence microscope located below the sample (Fig. 1(a)).

The two fluorescent molecules selected for this study are IR800cw carboxylate (Li-Cor), termed IR800cw (Fig. 1(c)) and indocyanine green (Sigma–Aldrich), termed ICG (Fig. 1(d)). The absorption and emission spectra of the two dyes, shown in Fig. 1(b), overlap well with the plasmon resonance from a 10 nm gap Au bowtie nanoantenna (black in Fig. 1(b)), so the bowtie would be expected to potentially enhance both the absorption and emission from these molecules when they are located in the gap between the two triangles of the bowtie [12].

The maximum fluorescence enhancement (f) possible for a particular dye molecule coupled to the enhanced gap region of the bowtie compared to an unenhanced single emitter is dependent upon the enhancement of the absorption of light (f_E) arising from locally enhanced pumping intensity as well as the enhancement or quenching of the fluorescence quantum efficiency (f_η) according to

$$f = f_E f_\eta$$

The enhancement of the light absorption process is simply dependent upon the change in the local pump intensity ($|E|^2$) due to the nanoantenna's presence and has been previously calculated using Finite-Difference Time-Domain (FDTD) simulations to be a factor of 180 when using 780 nm excitation wavelength for a molecule in the center of a 16 nm bowtie gap [12]. The change in the quantum efficiency (QE), however, is highly dependent upon the intrinsic QE of the molecule η_0 and other photophysical parameters according to [12]:

$$f_\eta = \frac{\eta'}{\eta_0} = \frac{\gamma'_r/\gamma_r}{1-\eta_0+\eta_0(\gamma'_r/\gamma_r+\gamma'_{nr}/\gamma_{nr})}$$

where η_0 is the molecule's intrinsic QE, η' is the molecule's QE when coupled to the bowtie, γ_r is the molecule's intrinsic radiative rate, and γ'_r and γ'_{nr} are the molecule's radiative and non-radiative rates when coupled to the bowtie. This function is plotted in Supplementary Fig. 1 using the FDTD-calculated values for γ'_r/γ_r and γ'_{nr}/γ_r. The point here is that a molecule with an already high QE cannot easily have its fluorescence emission enhanced, only its pumping rate. However, a molecule that has a low QE due to intrinsic nonradiative decay can have its emission enhanced, because the bowtie provides a much improved coupling to the far field by virtue of its ability to emit as a large dipole antenna driven by the oscillating molecular dipole, which increases the radiative rate. This works as long as the additional nonradiative decay channel provided by the Ohmic currents in the bowtie is not too large.

The best choice of molecule for high-concentration FCS experiments is a molecule that has the highest fluorescence enhancement. The η_0 of ICG in water is 2.4%, which corresponds to a maximum fluorescence enhancement of 1700 when the molecule is optimally located in the bowtie gap with absorption/emission dipole along the bowtie axis. The η_0 of ICG increases to 14% in ethanol, which corresponds to a much lower maximum fluorescence enhancement of 310, but allows for this molecule to be measured in typical no-bowtie FCS measurements as a control. Finally, the η_0 of IR800cw in ethanol is 28%, which means it will have an even lower maximum fluorescence enhancement of 157.

Bowtie nanoantennas are fabricated on indium tin oxide-coated glass substrates using E-beam lithography to have 70 nm sides, 20 nm thickness, and gaps near 20 nm as shown in the SEM in the inset of Fig. 1(b). In order to immerse the bowties in concentrated solutions of dye molecules, a simple fluid cell is constructed from 2 coverslips, one with the fabricated bowtie nanoantennas on the surface and the other unstructured with an o-ring sandwiched in between. The coverslips and o-ring were first cleaned in water and then ozone-cleaned for 10 min, before adding the concentrated dye solutions to form a sealed chamber above the bowtie.

Confocal fluorescence measurements of concentrated dye solutions on bowtie nanoantennas were performed using a home-built confocal microscope with 780 nm continuous wave pumping (10 ms/pixel; setup details: Supplementary Fig. 2). Fig. 2(a) and (d) are confocal images of IR800cw and ICG doped into 30 nm thick PVA films on top of an array of bowties (films were spin-cast from 2% PVA in water). These images reveal that the bowtie nanoantennas do enhance bulk fluorescence from these two molecules in

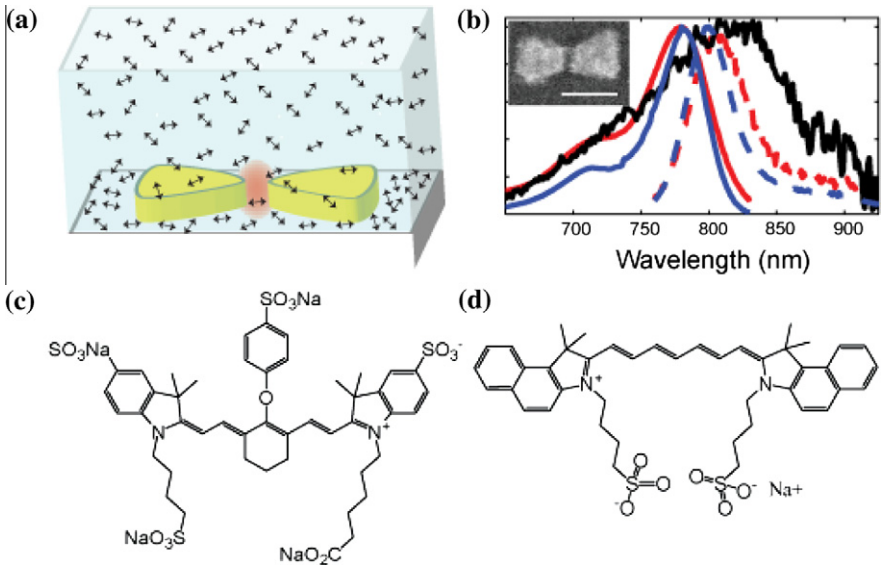

Fig. 1. (a) Bowtie nanoantennas are immersed in concentrated dye solutions for FCS experiments, shown schematically. (b) Blue – absorption (solid) and emission (dashed) spectra of IR800cw in ethanol. Red – absorption (solid) and emission (dashed) spectra of ICG in water. Black – plasmon resonance (scattering spectrum) of a 12 nm gap Au bowtie nanoantenna. Measured as in Ref. [18]. Inset: SEM of a typical gold bowtie nanoantenna. Scale bar = 100 nm. (c) ICG molecular structure. (d) IR800cw molecular structure. (For interpretation of the references to color in this figure legend, the reader is referred to the web version of this article.)

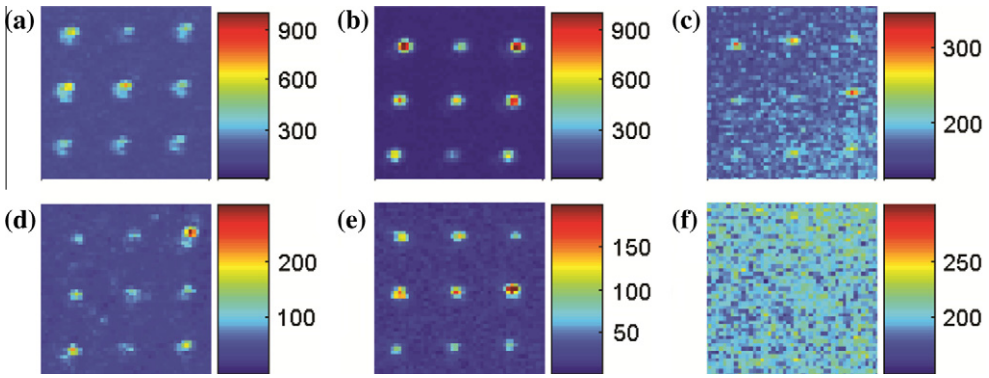

Fig. 2. Confocal images of an array of bowties in the presence of (a) 30 nm thick PVA film doped with IR800cw, 36 W/cm^2 imaging intensity, (b) 100 nM IR800cw in ethanol, 109 W/cm^2 imaging intensity, (c) 100 μM IR800cw in ethanol, 3 W/cm^2 imaging intensity, (d) 30 nm thick PVA film doped with ICG, 1.2 kW/cm^2 imaging intensity. (e) 1 μM ICG in water, 1.2 kW/cm^2 imaging intensity, (f) 1 μM ICG in ethanol, 600 W/cm^2 imaging intensity.

rigid polymer environments. Therefore, ICG and IR800cw are good candidate molecules to look for bowtie-enhanced fluorescence in solution.

Moving on to solution environments, at 1 μM concentration there are only 0.004 molecules/(20 nm)^3 region. Even with very few molecules present in the enhanced region on average, it is easy to see bright fluorescence spots from bowties immersed in an IR800cw solution (100 nM concentration in ethanol, Fig. 2(b)) and in an ICG solution (1 μM concentration in water, Fig. 2(e)), suggesting strong fluorescence enhancement is present. It is as if the molecules linger longer in the enhanced region. Here we show that the enhancement is actually due to molecules that transiently stick to the substrate surface instead of molecules floating in solution, a conclusion supported by several key pieces of experimental evidence. First, using separate observations of fluorescence from molecules in the presence of an ITO-coated surface without bowties, ICG was found to stick to the ITO surface in water but not in ethanol (Supplementary Fig. 4), and IR800cw sticks to the surface for either solvent. While bowties submerged in an ICG/water solution easily showed enhanced fluorescence (Fig. 2(e)), when the solvent is changed to the solvent that suppresses sticking (ethanol), the enhancement disappears (Fig. 2(f)). Second, the concentration dependence (Supplementary Fig. 3) suggests that the surface is nearly saturated with sticking molecules even at 100 nM concentration (Fig. 2(b)). This is also evident from signal-to-background considerations; bowties immersed in a highly concentrated solution of IR800cw (100 μM in ethanol, Fig. 2(c)) are only barely detectable above background. This implies that the gap region was already saturated with molecules on the surface at 100 nM concentration (100 nM in ethanol, Fig. 2(b)), so that by increasing the concentration by 1000×, only the background would increase. One might wonder if the highly anisotropic and concentrated optical field of the bowtie is producing some degree of trapping by gradient forces, but this is not consistent with the fact that as the optical intensity increases, the lingering time of molecules near the enhanced region drops (discussed in detail in Figs. 4 and 5 below).

It has been found that the Raman signal from molecules absorbed to small metal colloids can also be enhanced enough to be able to measure Raman scattering from single molecules [19]. Since the enhanced emission we observe originates from molecules stuck to either the substrate or the gold in the bowtie gap, it is necessary to rule out Surface Enhanced Raman Scattering (SERS) from local hot spots with extreme chemical enhancements [20]. SERS has a different spectral behavior as compared to fluorescence, so emission spectra were taken of the emission from both bulk and bowtie-enhanced molecules (Supplementary Fig. 5). The measured spectra are typical for room-temperature fluorescence measurements and do not show sharp features typically associated with Raman transitions in these molecules [21], effectively ruling out SERS effects.

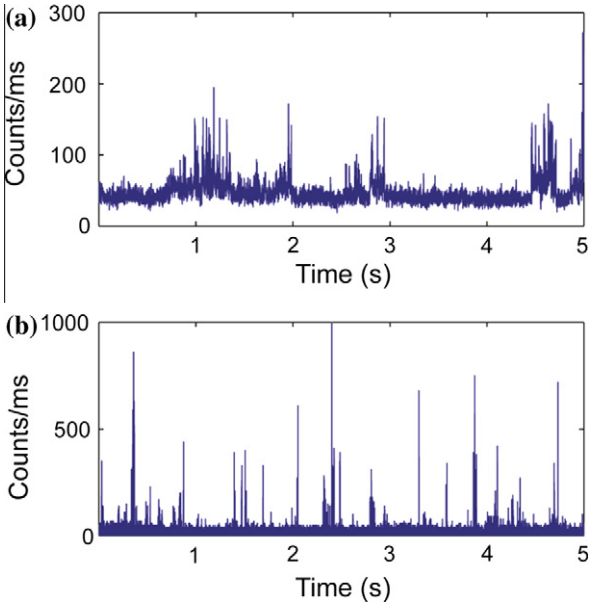

Fig. 3. Fluorescence time trace binned to 1 ms for a bowtie immersed in (a, upper curve) 1 μM IR800cw in ethanol using 430 W/cm^2 laser intensity and in (b, lower curve) 1 μM ICG in water using 144 kW/cm^2 laser intensity. ICG in water has higher contrast between enhanced molecules compared to background than IR800cw in ethanol.

Single-molecule information can be obtained from measurements of the emission in the time domain. Time traces of the fluorescence emission intensity for single bowties immersed in a 1 μM solution of IR800cw in ethanol and ICG in water are shown in Fig. 3. In both cases, bursts of fluorescence can be seen whenever a molecule enters the enhanced field region of the bowtie nanoantenna and until the molecule eventually photobleaches. No single-molecule fluorescence flashing events are measured in the absence of the bowtie nanoantennas at 1 μM concentrations of either dye, as is expected since with large numbers of the molecules N in the much larger diffraction-limited focal spot, the bursts cannot be observed above the background (and the contrast in the autocorrelation disappears, see below). Fig. 3 shows that the contrast between single enhanced molecules and background is much higher for ICG than for IR800cw. This difference supports the

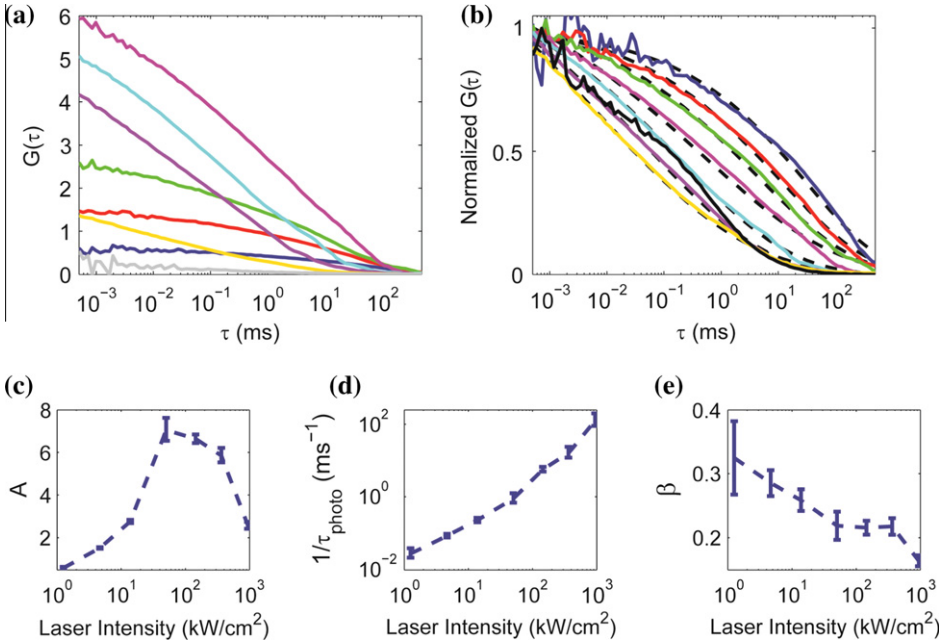

Fig. 4. (a) FCS curves for a bowtie immersed in a solution of 1 μM ICG in water when illuminated with pump intensity 1.3 kW/cm^2 (blue), 4.6 kW/cm^2 (red), 14 kW/cm^2 (green), 50 kW/cm^2 (pink), 144 kW/cm^2 (cyan), 362 kW/cm^2 (purple), and 940 kW/cm^2 (yellow). The gray curve indicates the FCS curve for the same 1 μM ICG in water solution but without a bowtie nanoantenna at 110 kW/cm^2 laser intensity. (b) FCS curves from (a) are normalized to their value at τ = 100 ns and clearly show that the photobleaching time, τ_{photo}, decreases as the laser intensity increases. Fits to each curve using the stretched exponential are plotted with dashed black lines. The FCS curve for a 10 pM solution of ICG in the absence of a bowtie nanoantenna with 2.9 MW/cm^2 laser intensity is plotted in solid black. (c)–(e) Fit parameters used for fit curves shown in (b) using the stretched exponential function in the text. (For interpretation of the references to color in this figure legend, the reader is referred to the web version of this article.)

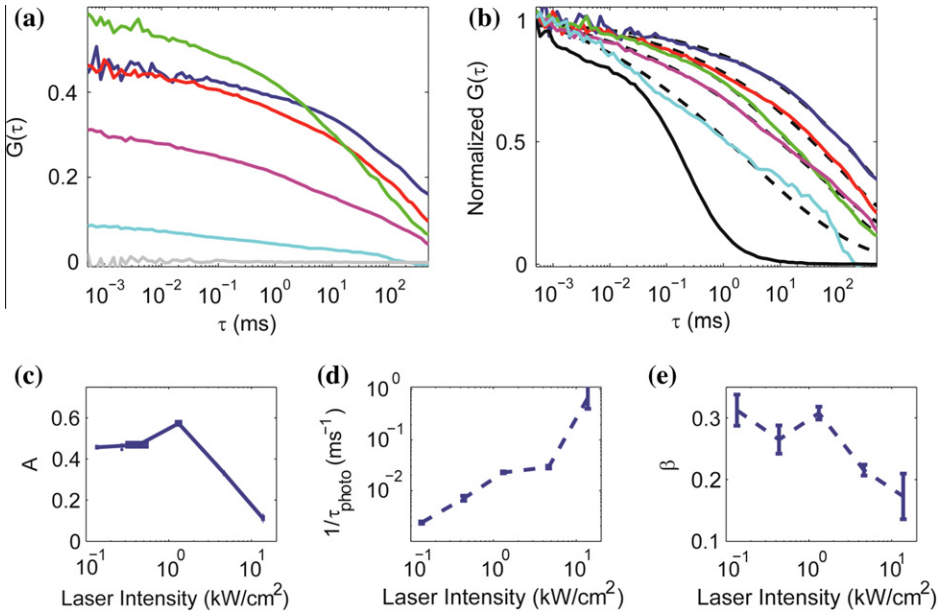

Fig. 5. (a) FCS curves for a bowtie immersed in a solution of 100 nM IR800cw in ethanol when illuminated with 0.14 kW/cm^2 (blue), 0.47 kW/cm^2 (red), 1.3 kW/cm^2 (green), 4.6 kW/cm^2 (pink), and 13.8 kW/cm^2 (cyan). The gray curve indicates the FCS curve for the same 100 nM IR800 in ethanol solution but without a bowtie nanoantenna at 1.3 kW/cm^2 laser intensity. (b) FCS curves from (a) are normalized to their value at τ = 100 ns and clearly show that the photobleaching time decreases as the laser intensity increases. Fits to each curve using a stretched exponential are plotted with dashed black lines. The FCS curve for a 10 pM solution of IR800cw in the absence of a bowtie nanoantenna with 1.9 MW/cm^2 laser intensity is plotted in solid black; the usual falloff from simple diffusion is clearly present. (c)–(e) Fit parameters used for fit curves shown in (b). (For interpretation of the references to color in this figure legend, the reader is referred to the web version of this article.)

conclusion that ICG is a better molecule for bowtie FCS than IR800cw since it has a lower intrinsic QE and hence a higher bowtie-induced fluorescence enhancement.

In a fluorescence correlation spectroscopy (FCS) experiment, the fluctuating fluorescence emission from a ultralow concentration dye solution irradiated by a focused laser beam is analyzed by calculating the autocorrelation function. Artifacts are avoided from APD detector dead times by using a 50/50 beamsplitter and two detectors and extracting the autocorrelation [3,22]

$$G(\tau) = \frac{\langle \delta I_1(t) \delta I_2(t+\tau) \rangle}{\langle I_1(t) \rangle \langle I_2(t) \rangle}$$

where $I_i(t)$ is the fluorescence intensity on one of the two detectors at time t and the numerator utilizes deviations from the average value in the calculation. The fluctuations can arise from diffusion as molecules move in and out of the focal volume or from internal dynamics of the emitter arising from triplet states, other dark states or even the excited state lifetime, but in standard FCS, the longest time scale addressed represents the time scale on which a molecule leaves the focal volume, usually on the order of 1 ms.

To characterize the standard unenhanced FCS curves for the two molecules, ITO-coated coverslips were used to support 10 pM solutions of ICG and IR800cw in ethanol, and the FCS curves show typical diffusion fall-off and short-time dynamics below 10 μs from intermediate states (Supplementary Fig. 6). ICG had to be measured in ethanol because the QE was too low to measure in water without the assistance of the bowtie nanoantenna. These curves are replotted in black in Figs. 4 and 5(b) for easy comparison with the bowtie-FCS data.

Fig. 4(b) shows normalized FCS curves for a variety of pumping intensities collected on a single bowtie immersed in 1 μM ICG in water. All FCS measurements were taken from 5 min of time-tagged fluorescence data, processed with the SymPhoTime package (Picoquant) and normalized to the value of $G(\tau)$ at τ = 100 ns. Notice that at lower excitation intensities, the timescale for the bowtie FCS curve decay is much longer than the FCS curve in the absence of the bowtie nanoantenna (black solid curve), opposite to the behavior one would expect from a falloff in correlation due to diffusion out of the tiny nanoscale gap region of the bowtie. This difference in time scale is consistent with the picture that molecules transiently stick to the surface near the bowtie nanoantenna and then photobleach. A light-dependent photoblinking process may also be involved, but for convenience below, we call the process photobleaching. The simplest model for photobleaching is that a molecule has a fixed probability of photobleaching during any excitation cycle and this does not change with excitation intensity. In practice, a molecule has a maximum total number of photons that it tends to emit on average before photobleaching, independent of excitation intensity over a large range. As the excitation intensity is increased, the molecule will emit the same total number of photons but in shorter periods of time, causing the photobleaching time, τ_{photo}, to shorten. This shortening of τ_{photo} is seen in the bowtie FCS curves in Fig. 4(b) as a shift of the FCS curves to the left at higher excitation intensities. Note that if there was a diffusion component to the FCS curve, it would not change with increasing power. This behavior is not observed, therefore the long-time decay in the bowtie FCS curves is not due to diffusion, but is instead due to the photobleaching behavior.

Since an enhanced molecule can be in a number of different positions and orientations on the surface near the bowtie gap and still contribute to the correlation, then a continuum of different photobleaching times must underlie the measured FCS curves. Photobleaching is often considered a Poisson process with exponential waiting time, but the bowtie's influence and the various orientations, etc. will create a distribution of characteristic times. The resulting multi-exponential behavior may be reasonably modeled with a stretched exponential [23,24]. Therefore, the bowtie FCS curves were fit with the following equation:

$$G(\tau) = Ae^{-(\tau/\tau_{photo})^{\beta}}$$

where A scales with the signal-to-background ratio (SBR), τ_{photo} is the photobleaching time parameter, and β is the stretching parameter. As with typical FCS, when β = 1, the FCS curve is a single exponential, but as β decreases below 1 toward zero, the exponential is stretched further and is representative of the sum of multiple exponentials. The fits agree well with the data and are plotted as dashed lines in Fig. 4(b). The extracted fit parameters are plotted in Fig. 4(c)–(e) as a function of pumping intensity with 95% confidence interval bootstrapped errors. In particular, notice that in Fig. 4(d) as the excitation power increases, $(\tau_{photo})^{-1}$ also increases, consistent with photobleaching behavior. For the bowtie FCS curves, β values between 0.15 and 0.32 are observed, indicating that the FCS curves are actually sums of a broad continuum of photobleaching times.

The amplitude of the decaying exponential (Fig. 4(c)) has interesting behavior because it is related to the single molecule signal–to-background ratio (SBR). In this case, the photons detected from the enhanced single molecule is the signal, while the background is a sum of photons from unenhanced molecules, ambient light leakage and dark noise from the detectors. At low excitation intensities, the background is dominated by ambient light leakage and dark noise, so by increasing the excitation intensity, the SBR goes up, as does the contrast in $G(\tau)$, visible also in the unnormalized data in Fig. 4(a). As the excitation is increased further, however, eventually the background from unenhanced molecules begins to dominate the background signal and lowers the SBR. Further, it is interesting to note that as the excitation intensity increases, β decreases (Fig. 4(d)), which suggests that at higher excitation intensities there are more underlying exponentials contributing than at lower excitation intensities. This indicates that more molecules in non-optimally orientations and locations contribute at higher excitation intensities.

Turning now to the other fluorophore, IR800cw, even though this molecule is not optimal for bowtie FCS, the bowtie FCS curves can still be recorded at low powers as shown in Fig. 5(a) and (b). Due to the higher η_0 of this molecule, the maximum bowtie-induced enhancement is lower which makes the FCS curves have lower contrast and thus more challenging to measure. Notice that the absolute G (100 ns) for these curves in Fig. 5(a) for IR800cw is much lower than in Fig. 4(a) for ICG, a consequence of a lower SBR for IR800cw. Similar trends are seen in the FCS fit parameters for ICG and IR800cw. As was measured for ICG bowtie FCS, the photobleaching time for IR800cw bowtie FCS is found to decrease as the excitation intensity increases (Fig. 5(d) and (b)). Also, the amplitude (A) of the fit first increases then decreases, although less dramatically than for ICG due to the higher η_0 of IR800cw. Finally, β also decreases, indicating a more stretched exponential, at higher excitation intensities.

In conclusion, bowtie FCS and the use of bowties to enhance fluorescence bursts from weak emitters has been shown to be a possible alternative to zero-mode waveguides when studying molecules immobilized on the surface of a substrate at high (μM) concentrations of fluorophore. As a proof-of-principle, bowtie FCS successfully measured the fluctuation dynamics of high (1 μM) concentrations of ICG in water as a function of laser intensity. While this method is currently limited to molecules that linger in the enhanced region due to transient sticking to the substrate, many experiments can be envisioned when alternate surface preparation and experimental design are used. For instance, an enzyme could be attached to the surface near the bowtie and whenever it acts on a fluorescently labeled substrate molecule at μM concentrations, then the molecule will be held near the bowtie for an extended period of time, allowing for easy measurement of its enhanced fluorescence. In a similar fashion, a biomolecule with a ligand binding site can be attached to the surface, and then fluorescently labeled ligands which bind to the biomolecule can be easily detected, and the unbinding times directly measured. With surface passivation to prevent sticking, the fluorescence bursts would be expected on a much faster time scale corresponding only to diffusion through the volume.

Acknowledgements

This work was supported in part by NSF Grant DMR-0507296 and by CPN through NSF Grant PHY-0425897 (WEM) and by an AFOSR MURI Program No. FA9550-04-1-0437 (SF).

Appendix A. Supplementary data

Supplementary data associated with this article can be found, in the online version, at http://dx.doi.org/10.1016/j.chemphys.2012.04.011.

References

[1] D. Magde, E. Elson, W.W. Webb, Phys. Rev. Lett. 28 (1972) 705.
[2] R. Rigler, E. Elson, Springer Ser. Chem. Phys. 65 (2001) 487.
[3] S.T. Hess, S. Huang, A.A. Heikal, W.W. Webb, Biochemistry 41 (2002) 697.
[4] P. Schwille, Cell Biochem. Biophys. 34 (2001) 383.
[5] J. Enderlein, I. Gregor, D. Patra, T. Dertinger, U.B. Kaupp, Chem. Phys. Chem. 6 (2005) 2324.
[6] F.J. Meyer-Almes, M. Auer, Biochemistry 39 (2000) 13261.
[7] M.J. Levene et al., Science 299 (2003) 682.
[8] J. Eid et al., Real-time DNA sequencing from single polymerase molecules, Science 323 (2009) 133–138.
[9] S. Uemura et al., Nature 464 (2010) 1012.
[10] J.A. Schuller et al., Nat. Mater. 9 (2010) 193.
[11] P.J. Schuck, D.P. Fromm, A. Sundaramurthy, G.S. Kino, W.E. Moerner, Phys. Rev. Lett. 94 (2005) 017402.
[12] A. Kinkhabwala et al., Nat. Photonics 3 (2009) 654.
[13] H. Aouani et al., ACS Nano 3 (2009) 7.
[14] D. Gerard et al., Phys. Rev. B 77 (2008) 045413.
[15] H. Rigneault et al., Phys. Rev. Lett. 95 (2005) 117401.
[16] J. Wenger, P. Lenne, Opt. Express 13 (2005) 7035.
[17] L.C. Estrada, P.F. Aramendia, O.E. Martinez, Opt. Express 16 (2008) 20597.
[18] D.P. Fromm, A. Sundaramurthy, P.J. Schuck, G.S. Kino, W.E. Moerner, Nano Lett. 4 (2004) 957.
[19] S. Nie, S.R. Emory, Science 275 (1997) 1102.
[20] M. Fleischmann, P.J. Hendra, A.J. McQuillan, Chem. Phys. Lett. 26 (1974) 163.
[21] J. Kneipp, H. Kneipp, W.L. Rice, K. Kneipp, Anal. Chem 77 (2005) 2381.
[22] J. Widengren, U. Mets, R. Rigler, J. Phys. Chem. 99 (1995) 13368.
[23] D.M. Burland, R.D. Miller, C.M. Walsh, Chem. Rev. 94 (1994) 31.
[24] L. Edman, U. Mets, R. Riger, Proc. Natl. Acad. Sci. USA 93 (1996) 6710.